3–20 GHz GaN MMIC Power Amplifier Design Through a COUT Compensation Strategy

3–20-GHz GaN MMIC Power Amplifier Design Through a C_{OUT} Compensation Strategy

Jorge Julian Moreno Rubio, Roberto Quaglia, *Member, IEEE*, Anna Piacibello, *Member, IEEE*, Vittorio Camarchia, *Senior Member, IEEE*, Paul J. Tasker, *Fellow, IEEE*, and Steve Cripps, *Life Fellow, IEEE*

***Abstract*— This letter presents the design approach for a compact, single-stage, wideband MMIC power amplifier. A method is proposed to compensate for the output capacitance of the active device over a frequency range as wide as possible, with minimum impact on the achievable output power, which leads to a two-element compensating network. A three-section transformer is then adopted for a real-to-real transformation. The CW characterization shows the output power higher than 32 dBm and the drain efficiency between 35% and 45%, over a fractional bandwidth of 148%, from 3 to 20 GHz.**

***Index Terms*— Broadband matching networks, FETs, gallium nitride (GaN), microwave amplifiers, wideband.**

I. Introduction

FUTURE high-performance broadband systems, such as RF and microwave front-end systems, radar, and software reconfigurable communication links, require wideband microwave monolithic integrated circuit (MMIC) power amplifiers (PAs). Gallium–nitride (GaN) high-electron-mobility transistors (HEMTs) are becoming the technology of choice for the PA due to their high power density at microwave frequencies. To achieve decade-bandwidth performance, distributed PAs are typically used, normally in a nonuniform topology to improve output power and efficiency [1]–[4]. Other wideband GaN PAs have been proposed, relying, for example, on reactive matching [5] or a reconfigurable dual-band operation [6], covering smaller bandwidths (6–18 GHz).

In this work, we propose a novel design strategy to compensate for the output capacitance C_{OUT} of the HEMT for any device size, as long as C_{OUT} is an accurate representation of the output reactive effects of the device. A 3–20-GHz single-ended MMIC amplifier fabricated on a 100-nm GaN-on-Si process is presented to demonstrate the validity of the approach. The results compare well with the state of the art (see Table I) while relying on a simpler design approach and using a single transistor and small MMIC area.

Manuscript received February 17, 2021; accepted March 2, 2021. Date of publication March 17, 2021; date of current version May 10, 2021. This work was supported in part by the European Union's Horizon 2020 Research and Innovation Programme through the Marie Sklodowska-Curie Agreement under Grant 793529. *(Corresponding author: Jorge Julian Moreno Rubio.)*

Jorge Julian Moreno Rubio is with the Centre for High Frequency Engineering, Cardiff University, Cardiff CF24 3AA, U.K., and also with the Research Group GINTEL, Universidad Pedagógica y Tecnológica de Colombia, Sogamoso 150003, Colombia (e-mail: jorgejulian.moreno@uptc.edu.co).

Roberto Quaglia, Paul J. Tasker, and Steve Cripps are with the Centre for High Frequency Engineering, Cardiff University, Cardiff CF24 3AA, U.K. (e-mail: quagliar@cardiff.ac.uk).

Anna Piacibello is with the Department of Electronics, Politecnico di Torino, 10129 Turin, Italy, and also with the Microwave Engineering Center for Space Applications (MECSA), 00133 Rome, Italy (e-mail: vittorio.camarchia@polito.it).

Vittorio Camarchia is with the Department of Electronics, Politecnico di Torino, 10129 Turin, Italy (e-mail: vittorio.camarchia@polito.it).

Color versions of one or more figures in this letter are available at https://doi.org/10.1109/LMWC.2021.3066282.

Digital Object Identifier 10.1109/LMWC.2021.3066282

II. Design

A. Optimal Load Identification

The optimal intrinsic load of an FET can be considered real and frequency-independent. However, the dispersion effects, which can be modeled with an equivalent output capacitance, make the extrinsic load strongly dependent on the frequency. The proposed PA design method shows a specific, simple way of compensating C_{OUT}, and then relies on a real-to-real transformation from the system impedance to the intrinsic optimum load.

In the estimation of the optimal extrinsic load, the device output capacitance C_{OUT} can be considered constant for the sake of simplicity [7], and it is estimated using Cold-FET simulations [8]. For the adopted device, a GaN-on-Si 100-nm gate-length 8×100 μm device supplied by OMMIC, the obtained value for C_{OUT} is 0.37 pF.

As a reference, an idealized output network is shown in Fig. 1(b). The negative capacitance would compensate for the effect of C_{OUT} at each frequency, and the resistor R_{opt} represents the optimal intrinsic load of the device. For this device, $R_{opt} \approx 20$ Ω, taking into account a drain-to-source bias voltage: $V_{DD} = 12$ V, knee voltage: $V_k = 2$ V, and maximum current: $I_M = 1$ A.

From Fig. 1(b), the optimal reflection coefficient Γ_{opt} is found to describe a constant conductance circle as a function of frequency, with the center in $-g_{opt}/(1+g_{opt})$ and the radius $1/(1+g_{opt})$, given by

$$\Gamma_{opt} = -\frac{g_{opt}}{1+g_{opt}} + \frac{1}{1+g_{opt}} e^{j2\arctan\left(\frac{2\pi f C_{OUT} Z_0}{1+g_{opt}}\right)} \quad (1)$$

where Z_0 is the reference impedance (50 Ω in this case), f is the frequency, and $g_{opt} = Z_0/R_{opt}$. Fig. 1(a) illustrates the arc that represents Γ_{opt} over a set of frequencies from dc to 25 GHz, which is obtained using (1).

The resistance $R_{opt} = 20$ Ω, as shown in Fig. 1(b), can be synthesized from the reference system impedance $Z_0 = 50$ Ω,

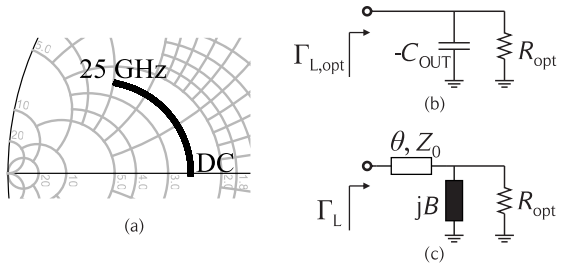

Fig. 1. Optimal load on (a) admittance Smith Chart, (b) ideal OMN, and (c) alternative OMN.

and with an arbitrary bandwidth, using a multisection transformer. In other words, the required bandwidth can be guaranteed for this transformation by using enough sections for the transformer. It is important, however, to balance the number of sections between transformation accuracy and inserted losses and size. If this can be achieved reasonably in the technology adopted, then the problem reduces to designing a network that synthesizes, as precisely as possible, the negative capacitance effect shown in Fig. 1(b).

B. Idealized Solution

In practice, the arc shown in Fig. 1(a) cannot be synthesized by a single passive element. However, using a two-element network, an approximated solution can be found. In order to estimate the limitations of a practical solution, an idealized solution, which follows perfectly Γ_{opt} in (1), is studied. As illustrated in Fig. 1(c), it is composed of a shunt susceptance B and a series transmission line of electrical length θ and characteristic impedance Z_0, where

$$B = \omega C_{OUT} \tag{2}$$

and

$$\theta = \arctan\left(\frac{-2BY_0}{Y_0^2 - G_{opt}^2 - B^2}\right) \tag{3}$$

with $\omega = 2\pi f$, $Y_0 = 1/Z_0$ and $G_{opt} = 1/R_{opt}$.

Equation (2) suggests that the most trivial implementation of the shunt susceptance is adopting a capacitor (C_{OUT}). However, if B is linearly dependent on frequency, from (3), it follows that the electrical length θ is not linear with frequency. This is a significant practical limitation, given the linear frequency dependence of the electrical length of transmission lines.

However, as a tradeoff, an open stub can be used to synthesize B instead of a capacitor. Thus, B has a tangent-like dependence on frequency, which makes θ almost linear with frequency, as shown in the example of Fig. 2 and, therefore, better approximated by a common transmission line. Fig. 2 shows the frequency dependence of θ obtained using (3) for two cases, namely, using the ideal capacitor solution for B (2) and using an open stub.

C. OMN Design

Thus, assuming that R_{opt} is realized using a multisection transformer, the proposed OMN is shown in Fig. 3(a).

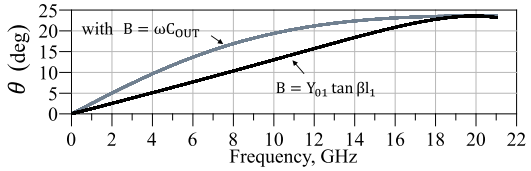

Fig. 2. Solution for (3) in two cases: B synthesized by a capacitor (gray) and by an open stub (black).

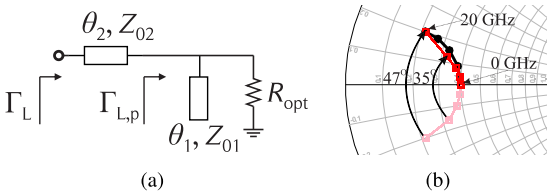

Fig. 3. (a) Proposed OMN and (b) Γ_L obtained with open stub (red), Γ_{opt} (black), and $\Gamma_{L,p}$ (pink).

The reflection coefficient $\Gamma_{L,p}$, obtained at the reference plane right after the stub, can then be expressed as

$$\Gamma_{L,p} = -\frac{g_{opt}}{1+g_{opt}} + \frac{1}{1+g_{opt}} e^{-j2\arctan\left(\frac{Z_0 \tan\theta_1}{Z_{01}\left(1+g_{opt}\right)}\right)}. \tag{4}$$

Equation (4) represents an arc similar to (1) but mirrored with respect to the real axis of the Smith Chart [see Fig. 3(b)]. Adding a series transmission line in front of the stub, as illustrated in Fig. 3(b), the group of points represented by $\Gamma_{L,p}$ turns clockwise on the Smith Chart, with an angle proportional to the frequency. Thus, assuming that $Z_{02} = Z_0$, the expression for Γ_L in Fig. 3(a) is given as follows:

$$\Gamma_L = e^{-j2\theta_2}\Gamma_{L,p}. \tag{5}$$

Using (5), a solution for θ_2 and θ_1 can be found, aiming to keep Γ_L close to Γ_{opt}. In general, the value of Z_{01} can be used as an optimization parameter to be selected before solving (5). In this case, for simplicity, $Z_{01} = Z_{02} = Z_0 = 50\ \Omega$.

Since the condition $\Gamma_L(0\text{GHz}) = \Gamma_{opt}(0\text{GHz})$ is guaranteed according to our assumptions, and the susceptance is expected to decrease with frequency in both cases, a convenient solution for θ_2 and θ_1 can be obtained solving $\Gamma_L(f_h) = \Gamma_{opt}(f_h)$, where f_h is a design parameter.

In order to select the value of f_h, the magnitude of the intrinsic load impedance $Z_{int} = 1/(Y_L + j\omega C_{OUT})$ can be observed over frequency. Thus, based on the bandwidth estimation method proposed in [9], the output power can be estimated as follows:

$$P_{OUT} = \begin{cases} \dfrac{1}{8} I_M^2 \Re\{Z_{int}\}, & \text{if } f \le f_h \\ \dfrac{1}{2}(V_{DD} - V_k)^2 \Re\left\{\dfrac{1}{Z_{int}}\right\}, & \text{if } f > f_h. \end{cases} \tag{6}$$

The difference between the estimated saturated power P_{OUT} and the maximum expected power from the device assumed as $P_{MAX} = 0.125 I_M^2 R_{opt} = 2.5$ W, for different choices of f_h, is shown in Fig 4. In this case, targeting for a maximum power reduction over the band lower than 0.7 dB, f_h is selected to be 20 GHz, obtaining $\theta_2 = 23.6°$ and $\theta_1 = 66.8°$ at 20 GHz. Fig. 3(b) shows how the series transmission line

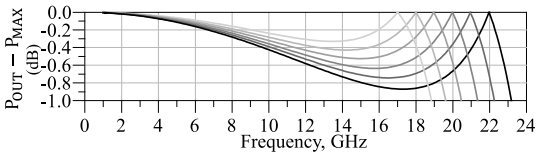

Fig. 4. Estimated output power for different values of f_h.

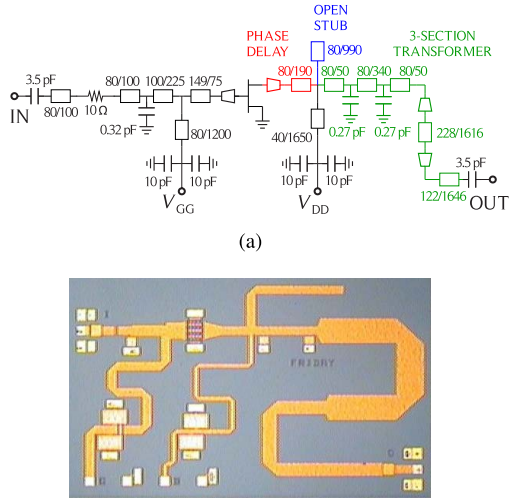

(a)

(b)

Fig. 5. Schematic (line dimensions are given as width/length in μm), device size: 8×100 μm, with (a) 100-nm gate-length and (b) picture of the realized wideband PA. The chip size is 3 mm $\times$ 2 mm.

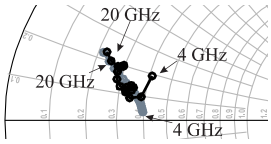

Fig. 6. Synthesized load $\Gamma_{L,syn}$ (black) and theoretical load Γ_L (gray).

produces different phase delays for different frequencies, and how, in this way, the synthesized reflection coefficient Γ_L can follow Γ_{opt} closely.

III. Realization and Characterization

Fig. 5(a) illustrates the final schematic of the designed PA, and its picture is shown in Fig. 5(b). The 20-Ω resistance is obtained through a three-section Chebyshev transformer centered at 15.5 GHz. The open-circuited stub is finely tuned to compensate for the reactive effect of the high impedance bias-tee included in parallel. The series transmission line is implemented including a taper that fits with the device drain pin width. The load $\Gamma_{L,syn}$ synthesized by the OMN is compared to the theoretical one in Fig. 6, highlighting the good agreement between 5 and 20 GHz. As expected, the differences at the lowest frequencies are due to the inclusion of the bias-tee and dc blocking capacitors.

The IMN has been designed to optimize the transducer gain over the band. A resistor has also been included for out- and in-band stabilizations.

The scattering and CW characterization results over the band of interest are shown in Fig. 7. The on-wafer calibration at the probe tips has been used, while an extended coaxial port calibration has been adopted to enable the power calibration using a power meter. The achieved bandwidth is in line with

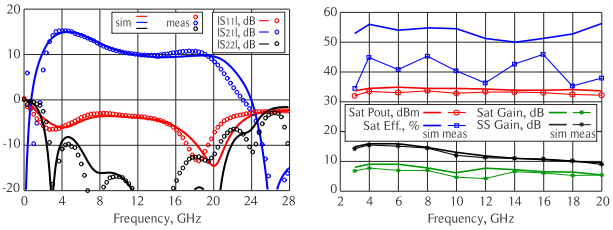

(a) (b)

Fig. 7. Comparison of simulated (solid) and measured (symbols): (a) $S_{1,1}$ (red), $S_{2,1}$ (blue), and $S_{2,2}$ (black) and (b) saturated output power (red), small-signal gain (black), saturated gain (green), and saturated efficiency (blue).

TABLE I
State-of-the-Art of Microwave GaN Wideband PAs

Ref.	Year	Area (mm^2)	BW (GHz)	BW (%)	Gain (dB)	P_{OUT} (dBm)	PAE (%)
[1]	2009	15	1.5–17	167	10–14	>39.6	20–38
[2]	2011	38	2–20	165	9–15	>40	15–36
[3]	2019	7.5	2–20	163	16–17.5	>33.8	18–37
[4]	2019	7	2–18	160	28–30	>39.6	18–38
[5]	2013	12	6–18	100	20–26	>40	10–25
[6]	2018	5.1	6–18	100	15–27	>34	15–34
This work	**2020**	**6**	**3–20**	**148**	**9–16**	**>32**	**27–38**

the expected one, apart from a slight shift, which affects the upper band edge. A saturated drain efficiency between 35% and 45% has been obtained over 17 GHz of bandwidth, from 3 to 20 GHz. The corresponding PAE ranges from 27% to 38%, while the obtained saturated output power is higher than 32 dBm over the band, and the power gain is between 9 and 16 dB. Table I shows that the results are comparable to the state of the art while using a simple design approach and a small-size MMIC. The measured results are in rather good agreement with the simulations, except for the discrepancy in the saturated efficiency, which can be justified both by the CW measurements being carried out on wafer directly on a room temperature chuck, without dedicated die attachment, and by the fact that load-pull measurements on the same device have shown the large-signal model to overestimate both saturated power and efficiency [10].

IV. Conclusion

A compact multioctave MMIC PA has been designed through a simple output capacitance compensation strategy. The obtained drain efficiency is shown to be between 35% and 45% over a 148% fractional bandwidth and with 32 dBm of the output power, in line with state-of-the-art broadband PAs for RF and microwave front-end systems.

References

[1] C. Campbell *et al.*, "A wideband power amplifier MMIC utilizing GaN on SiC HEMT technology," *IEEE J. Solid-State Circuits*, vol. 44, no. 10, pp. 2640–2647, Oct. 2009.

[2] J. J. Komiak, K. Chu, and P. C. Chao, "Decade bandwidth 2 to 20 GHz GaN HEMT power amplifier MMICs in DFP and no FP technology," in *IEEE MTT-S Int. Microw. Symp. Dig.*, Jun. 2011, pp. 1–4.

[3] M. Roberg, S. Schafer, O. Marrufo, and T. Hon, "A 2–20 GHz distributed GaN power amplifier using a novel biasing technique," in *IEEE MTT-S Int. Microw. Symp. Dig.*, Jun. 2019, pp. 694–697.

[4] H. Wu, Q. Lin, L. Zhu, S. Chen, Y. Chen, and L. Hu, "A 2 to 18 GHz compact high-gain and high-power GaN amplifier," in *IEEE MTT-S Int. Microw. Symp. Dig.*, Jun. 2019, pp. 710–713.

[5] U. Schmid *et al.*, "Ultra-wideband GaN MMIC chip set and high power amplifier module for multi-function defense AESA applications," *IEEE Trans. Microw. Theory Techn.*, vol. 61, no. 8, pp. 3043–3051, Aug. 2013.

[6] K. Choi, H. Park, M. Kim, J. Kim, and Y. Kwon, "A 6–18-GHz switchless reconfigurable dual-band dual-mode PA MMIC using coupled-line-based diplexer," *IEEE Trans. Microw. Theory Techn.*, vol. 66, no. 12, pp. 5685–5695, Jun. 2018.

[7] J. J. M. Rubio, R. Quaglia, A. Baddeley, P. J. Tasker, and S. C. Cripps, "Design of a broadband power amplifier based on power and efficiency contour estimation," *IEEE Microw. Wireless Compon. Lett.*, vol. 30, no. 8, pp. 772–774, Aug. 2020.

[8] Y.-L. Lai and K.-H. Hsu, "A new pinched-off cold-FET method to determine parasitic capacitances of FET equivalent circuits," *IEEE Trans. Microw. Theory Techn.*, vol. 49, no. 8, pp. 1410–1418, Aug. 2001.

[9] J. J. M. Rubio, V. Camarchia, R. Quaglia, E. F. A. Malaver, and M. Pirola, "A 0.6–3.8 GHz GaN power amplifier designed through a simple strategy," *IEEE Microw. Wireless Compon. Lett.*, vol. 26, no. 6, pp. 446–448, Jun. 2016.

[10] R. Quaglia *et al.*, "Source/load-pull characterisation of GaN on Si HEMTs with data analysis targeting Doherty design," in *Proc. IEEE Topical Conf. RF/Microwave Power Modeling Radio Wireless Appl. (PAWR)*, Jan. 2020, pp. 5–8.